Neutronics Aspects of the FESS-FNSF

A. Davis[a,*], M. Harb[a], L. El-Guebaly[a], P. Wilson[a], E. Marriott[a], FESS-FNSF team

[a] *1500 Engineering Drive, Madison, WI 53706*

Abstract

Neutronics analysis was performed on the latest Fusion Energy System Studies - Fusion Nuclear Science Facility (FESS-FNSF) design which covered the neutron wall loading, tritium breeding ratio, radiation damage, and shutdown dose rate calculations. Sixteen different sectors configurations were investigated with a main focus on determining the impact which each has upon the tritium breeding ratio (TBR) of the whole facility. This paper describes the stages of the nuclear analysis that serve to prove the radiation derived attributes of the system.

Keywords: FESS-FNSF, tritium breeding ratio, radiation damage, shutdown dose rate, DAGMC

*Corresponding author

List of Figures

1. Introduction

The Fusion Energy Systems Studies - Fusion Nuclear Science Facility (FESS-FNSF [1]) is considered an essential element of the US fusion road map that displays a strategic pathway from ITER, to US DEMO, and eventually to the first commercial power plant. A FNSF will help bridge the research gap between ITER - low radiation damage, short pulses, no tritium breeding - and DEMO which is designed to operate at power plant relevant fusion parameters. The FNSF will advance the understanding of fusion nuclear sciences (FNS) by providing an integrated platform for establishing a database on all components up to relevant parameters (e.g. 40-60 dpa, blanket temperatures 500-600°C) via in-depth investigation of issues related to plasma boundary interface (materials interaction with high energy neutron flux, surface/volumetric heating, radiation damage, and gas production), operating in power plant relevant fusion core conditions (temperatures, coolant/breeder flow rates, pressures/stresses, B-field, and neutrons), tritium breeding/extraction/processing, advancing and demonstrating plasma technologies that support very long duration operations, etc.

The FNSF subjected to this study is a tokamak-based facility with a 518 MW fusion power, a plant Lifetime $\sim$ 24 years ($\sim$ 8.5 FPY) and $\sim$ 35% availability. The machine average neutron wall loading (NWL) at the first wall is 1.1 MW/m^2. The radiation damage to the first wall was calculated followed by a shielding analysis. Shielding optimization [2] involved testing the effect of the inboard shielding materials on the radiation damage levels at the magnet with an inboard breeding blanket and the results showed that the radiation levels at the magnet are within acceptable limits. Such calculations involved estimating the fast neutron fluence, nuclear heating at the coil case, and atomic displacement to the Cu stabilizer.

A detailed tritium breeding study was also performed to assess the effect of various design elements on the tritium breeding ratio (TBR) of the dual-cooled lithium lead (DCLL) blanket which confirmed tritium self-sufficiency, a value of TBR $\sim$ 1 with 4% margin. Following the TBR calculations, shut-down dose rate analysis was performed which involved irradiation of one sector in the model (without any penetrations or ports) with a simplified irradiation scenario. The operation of the facility was assumed to be at a constant flux levels for 4.2 years followed by a complete shut-down. The dose

rate was estimated at 0 s, 1 d, 2 d, 7 d, 14 d, 0.1 y, and 0.25 y following the shut-down.

In section (2) the software tools used in this study will be described and in section (3) NWL results will be introduced. In section (4) focus will be on the tritium breeding calculations. In section (5) magnet shielding and radiation damage calculations will be discussed and finally in section (6) the shut-down dose rate calculations will be presented.

1.1. Configuration

The first step in the analysis involved optimization of the OB & IB radial builds and the divertor vertical build [2]. The result of such 1-D extensive optimization analysis is a complete definition of the material composition of the different regions taking into account the configuration of the facility, radiation limits especially at the magnet (and other long lifetime components), selection of low activation materials, environmental and safety constraints, and temperature limits for several in-vessel components. Some design parameters were pre-set based on decisions made during previous studies such as ARIES-ACT2 [3]. Such parameters included the sizes of the He-cooled 20 cm thick SR and 10 cm thick VV (both of these structures are composed to 2 face sheets with internal ribs and filler materials). As will be discussed in section (5) the most important parameters in the analysis were the fast neutron fluence and nuclear heating at the toroidal field magnet. The OB radial build and the corresponding material composition of each layer is shown in figure 1 and the detailed composition of the OB is;

100 cm	**2 mm W armor**	91.3% W, 8.7% void
	3.8 cm FW	34% FS (F82H), 66% He
	94 cm Breeding Zone	73.7% LiPb (90% Li-6), 14.9% He/void, 7.5% FS, 3.9% SiC
	2 cm Back Wall	80% FS, 20% He
	2 cm Stabilizing Shells	100% W alloy
	6 cm He Manifolds	30% FS, 70% He
	20 cm Structural Ring	28% FS, 20% He, 52% B-FS Filler
	10 cm VV	60% 3Cr-FS, 40% He
	17 cm LT Shield	39% 3Cr-FS, 29% B-FS, 32% H_2O
	Coil Case	100% SS-316LN
	Winding Pack#	30% JK2LB Steel, 25% Cu, 25% Ternary Nb_3Sn, 10% Hybrid Electric Insulator, 10% Liquid He

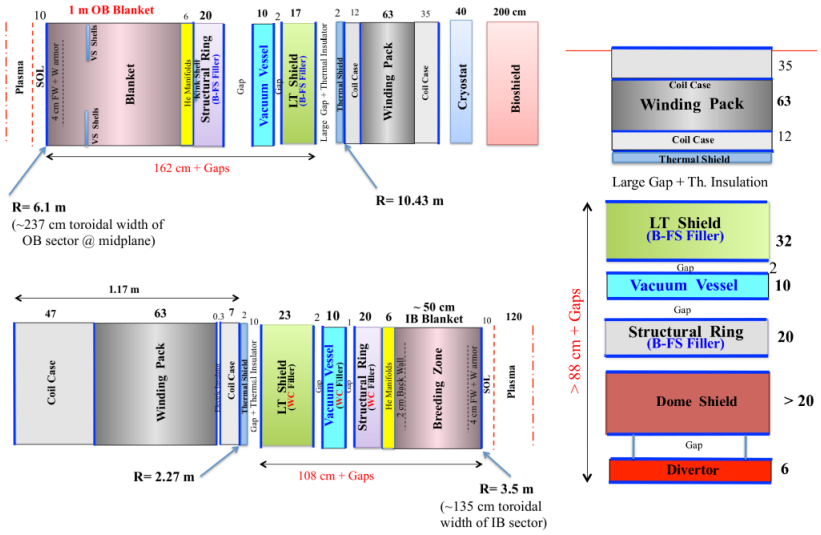

Figure 1: OB "top left", IB "bottom left", and Divertor "right" radial builds

1.2. Full 3D Build

The shielding and blanket optimization described in subsection (1.1) resulted in a full definition of the major materials and dimensions that were used to produce the 3D assembly CAD model. Shown in Figure 2 is a cross section of one sector with the major regions identified on the figure. The model consists of 16 IB and OB sectors with 2 cm assembly gaps which is used in all analyses performed in this study; TBR, Radiation damage and shutdown dose rate calculations. The facility has a major radius of 4.8 m and a minor radius of 1.2 m. It's worth mentioning that the CAD used in the analysis included all in-vessel components up to the IB magnet and out-of-vessel components up to the LT shield.

2. Analysis Tools

As will be discussed in section (4), calculation of the TBR with high fidelity has to be achieved in order to confirm the adequacy of the configuration of the facility for tritium self-sufficiency. Based on previous analyses, some margins are considered in the design phase such that the final integration of

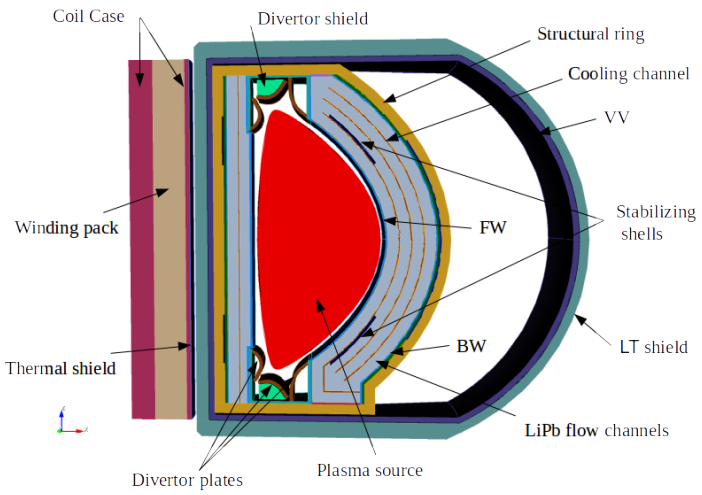

Figure 2: The full 3D CAD model of a single FESS-FNSF sector

all engineering systems in the facility will ensure a TBR > 1. One of the margins [4] considered in the design phase of the facility is directly related to deficiencies in modelling resulting from approximations introduced to facilitate the analysis especially the neutron/photon transport calculations.

In this study the approximations were limited and only applied to design details which are known – based on accumulated experience with previous models - to be of less importance regarding neutron/photon transport calculations besides slowing down the simulations if included. Such design details include; the detailed structure of the first wall "FW" and its He cooling system, the internal structure of the blanket cooling channels, and the internal structure of the He manifolds. Those regions are known to show little/no difference if modelled in detail or homogenized with a proper assignment of volume averaged material compositions.

State-of-the-art analysis tools were utilized in this study which enabled

working with the full 3-D model with all the internal details defined in the CAD, such as blanket internals and side/back/front walls, which are known to play a key role in TBR degradation. This work was performed with DAG-MCNP5, a version of MCNP5 [5] that has been enhanced by the DAGMC [6] toolkit. Coupled with MCNP5, DAGMC provides remarkable capabilities for the analysis of complex fusion facilities by utilizing acceleration techniques to achieve efficient ray tracing directly on CAD solid models without the need to translate the geometry/model to the native input representation of the transport code. Other software tools were used for mesh representation of the geometry and application of transport variance reduction techniques for deep penetration in regions behind the shields (PyNE [7] toolkit). The fusion evaluated nuclear data library (FENDL2.1)[8] was used in this analysis. Utilization of such sophisticated tools allowed reducing the approximations involved in the analysis by incorporating fine details which previously represented a challenge.

The Shut-down dose rate (SDDR) analysis of the facility also plays a key role in the design phase. In the current study the r2s [9, 10] workflow was used to perform the activation and shut-down dose rate calculations in one sector (without any penetrations or ports) of the facility with a simplified irradiation scenario. The analysis involved performing neutron transport calculations followed by nuclear inventory analysis using ALARA [11] code and then finally a photon transport step using the produced decay gamma sources distribution for sampling.

2.1. Neutron Source Modeling

An MCNP sampling routine was written to sample the neutrons for the transport calculations compared to the previous workflow which utilized either a simplified 3-region or R-Z sources. It has been shown by mapping the neutron source using different source definitions that the method by which neutrons are sampled from the source will have an impact on the analysis results such as NWL and hence TBR and radiation damage values. such difference is directly related to the source configuration which affects, for example, the peaking values at the mid-plane. Advances in Modelling allowed a transition from a 3-region (concentric three tori with different neutron yield) to sampling based on produced R-Z source density distribution to sampling the source as a function of the actual parameters defining the plasma without the need to introduce any approximations. The new routine

also samples the energy of the neutrons over a Gaussian/Muir distribution rather than a fixed value (check and elaborate!). The physical parameters defining the plasma source [12] are: fusion power = 518 MW, major radius = 4.8 m, minor radius = 1.2 m, elongation = 2.2, triangularity = 0.625, Shafranov shift = 0.144 m, ion density in the pedestal, seperatrix, and core regions = $1\text{x}10^{20}/\text{m}^3$, $0.56\text{x}10^{20}/\text{m}^3$, and $1.6\text{x}10^{20}/\text{m}^3$ respectively with a peaking factor of 1.52 (peak to volume average), ion temperature in the pedestal, seperatrix, and core regions = 4 keV, 100 eV, and 22 keV respectively with a peaking factor of 2.25 (peak to volume average), and pedistal radius = 1.14 m.

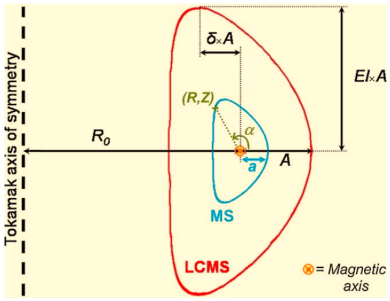

Figure 3: The analytic source configuration

3. Neutron Wall Loading

The next step in the analysis was applied to the full 3-D model which involved calculations of the NWL distributions at the IB & OB FWs, the inner & outer divertor plates, and the middle divertor plate (dome). The vertical distribution of the NWL at the FWs (figure 5) and inner & outer divertor plates (figure 6) were calculated over segments ~ 10 cm high starting from the mid-plane and moving upward. It's worth noting that the NWL was calculated at the FW and not over any approximated contour and the segments used in the calculations are shown in figure 4 for the top half of the model. The radial distribution of the NWL at the dome is shown in figure 7. Table 1 shows the calculated peak and average values at the FWs and divertors. The average values are area avergaes over each surface of the corresponding region. The peak values at the FWs occur at the mid-plane while for the inner and outer divertors it occurs at the bottom portion of the

plates where it's closer to the plasma source. For the dome the peak value occurs in the middle.

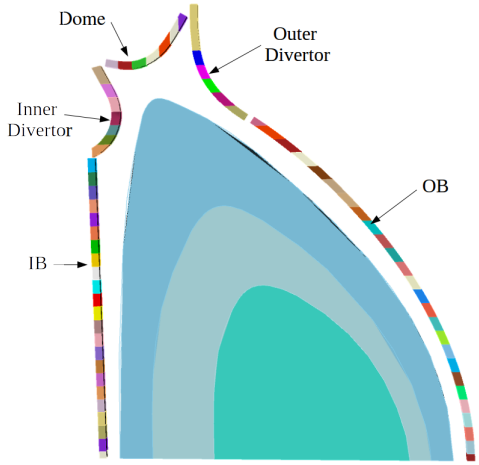

Figure 4: OB, IB, and Divertor segments used in NWL analysis

Table 1: NWL peak and average values

	Peak NWL [MW/m^2]	Average NWL [MW/m^2]
OB FW	1.75 ± 0.11%	1.35
IB FW	1.31 ± 0.17%	0.86
Inner Divertor	0.79 ± 0.25%	0.32
Dome	0.66 ± 0.27%	0.49
Outer Divertor	0.76 ± 0.14%	0.35
all 3 Divertor plates	0.79 ± 0.13%	0.38

4. Tritium Breeding Calculations

The rich fusion research literature shows a growing interest to achieve ignition via the deuterium - tritium (D-T) fuel cycle and due to the scarcity of T in nature and the high cost of T consumed by fusion power plants (55.6 kg/full power year (FPY)/GW$_{fus}$) [4], all power plants developed to date that employ the D-T fuel cycle are required to breed T in blankets surrounding the plasma. As a result the need for TBR (ratio of tritium bred in the blankets to that consumed in the plasma) calculations with high

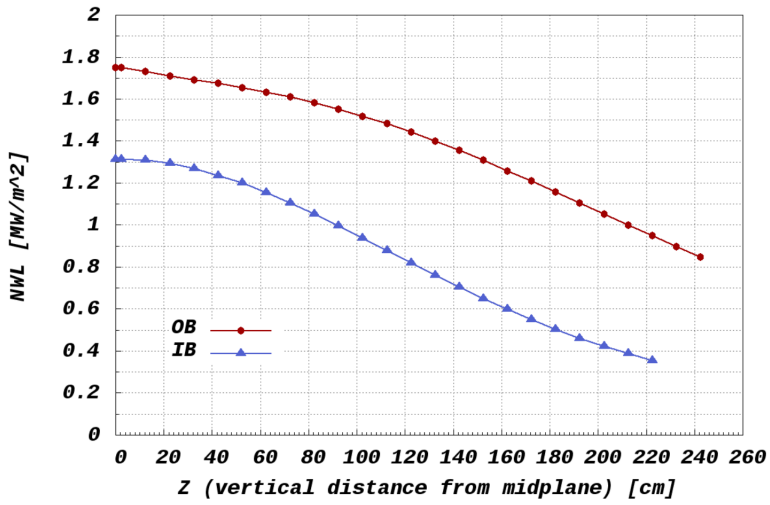

Figure 5: The NWL vertical distribution at IB & OB FW

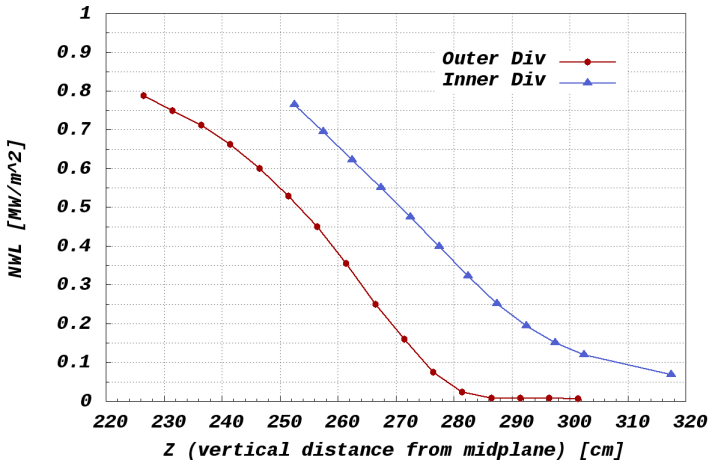

Figure 6: The NWL vertical distribution at the inner and outer divertors

certainty grew substantially and the TBR is considered an essential metric in the design phase.

The blanket of choice for the FESS-FNSF project is the dual cooled lead-lithium (DCLL) [13] blanket. The blanket consists of ~ 20 cm radial/toroidal flow channels of LiPb eutectic (15.7 at% Li (90% Li6 enrichment) and 84.3

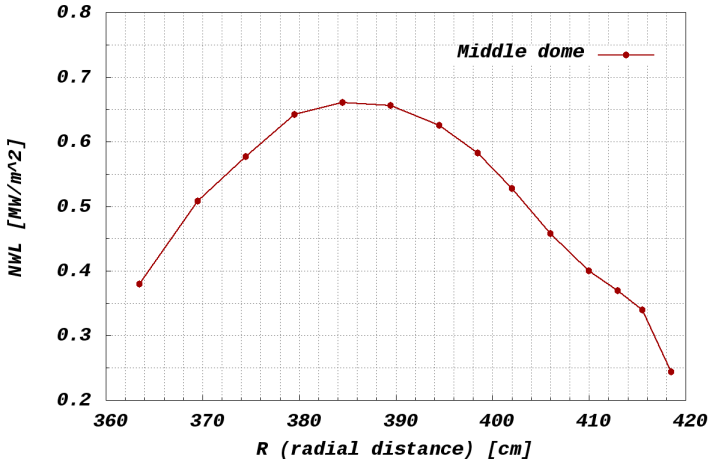

Figure 7: The NWL distribution at the dome

at% Pb) surrounded by 0.5 cm SiC FCI (flow channel insert) and 0.2 cm layer of LiPb. The blanket structure is cooled by helium at high pressure (8 MPa) which is also used for heat removal in other components such as FW and blanket side/back/front walls. The blanket also serves other purposes besides breeding T such as the removal of volumetric heat deposited by fast neutrons from the plasma and shielding the outer components such as the structural ring (SR), the vacuum vessel (VV), and the magnets.

4.1. TBR Workflow

A workflow for the calculation of the TBR of the facility was developed which involved assessing the impact of individual design elements/details on the breeding capacity. The workflow consists of a multi-step approach to calculate the TBR by starting the analysis with a CAD model with a simplified breeding blanket and at each step a new detail is added such as the He flow channels, the side walls, etc. and the resulting TBR of the facility is calculated at each step. The TBR results are shown in figure 8.

Step 1 is a reference case showing the TBR for an infinite cylinder of LiPb surrounded by shields with a coaxial plasma source. The calculated value represents the maximum achievable TBR for a hypothetical infinite medium. In step 2, the model was constructed of 16 sectors each consisting of IB and OB breeding blankets surrounded by shields and divertors with

2 cm assembly gaps between the sectors. The 3-D configuration with such radial and poloidal coverage (compared to the infinite case in step 1) resulted in a TBR drop of 19.74%. The assignment of the homogenized composition (34% ferritic steel (FS), 66% He) to the 3.8 cm thick IB and OB FWs in all sectors (step 3) resulted in a TBR drop of 8.7%. Modeling of side walls (same thickness and composition as FW) and the 2 cm thick back walls (80% FS, 20% He) in all sectors (step 4) resulted in an additional TBR drop of 2.79%. Defining the main LiPb flow channels by modelling the 1.5 cm cooling channels with an assigned composition (58% FS, 42% He) in all sectors (step 5) resulted in a further drop of 3.95%. Assigning 34% SiC to the 0.5 cm FCI in all sectors (step 6) resulted in a drop of 4.6%. Adding the 2 cm IB and OB stabilizing shells (W alloy) to all sectors (step 7) resulted in a drop of 4.11%.

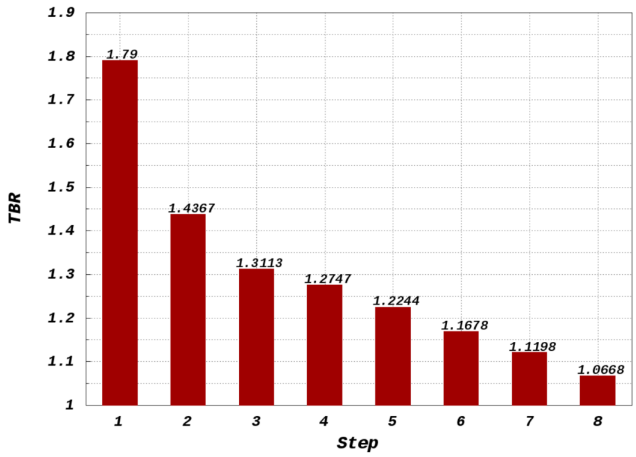

Figure 8: TBR chart

4.2. Penetrations and Ports

The facility has 12 mid-plane and 6 off-mid-plane ports, the effect of which was assessed by adding each type of ports to the respective sectors (for analysis purposes) and calculate the facility overall TBR and the corresponding drop (compared to step 7). It's worth noting that the ports were modelled in detail; frames, gaps, blanket frames, and internal structures were included in the CAD model. Adding the material testing module (MTM) to

1 sector (1 m^2 at FW) resulted in a drop of 0.313%. The facility has 4 testing blanket modules (TBM) (in 4 sectors, 1 m^2 each at FW), for purposes of testing different breeding concepts, resulting (all four TBMs) in a drop in the TBR of 0.2%. The three plasma diagnostics ports resulted in a drop of 0.95%. Including two neutral beam injectors (NBI) (in 4 sectors, 1.9 m^2 each at FW) reduced the TBR by 1.63%.

The remaining ports; IC (in 1 sector, 2 m^2 at FW), LH (in 1 sector, 1.5 m^2 at FW), EC (in 1 sector, 0.675 m^2 at FW), Fueling (in 1 sector, 0.04 m^2 at FW), Disruption mitigation (in 1 sector, 0.04 m^2 at FW), and two Divertor diagnostics (in 1 sector, 0.15 m^2 each at FW) resulted in a TBR drop of 0.71%, 0.5%, 0.23%, 0.02%, 0.02%, and 0.08%, respectively. A final step (step 8 on figure 8) with all penetrations included at the same time resulted in a drop of 4.95%. A planar cross section of the facility with all penetrations identified is shown in figure 9.

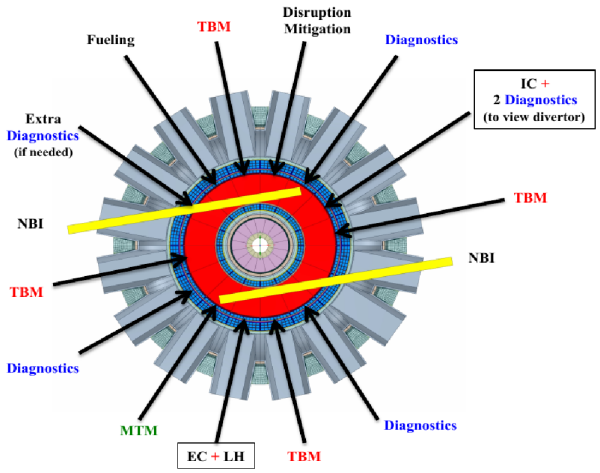

Figure 9: Cross-section of the facility at the mid-plane

4.3. Li-6 Enrichment

One of the advantages of the DCLL blanket is allowing the control of the T bred by controlling the Li^6 enrichment in LiPb in the main flow channels. Controlling Li^6 enrichment is necessary to avoid dealing with a surplus or shortage of T. Analyses were performed to test the effect of changing Li^6 enrichment on the overall TBR of the facility (with all penetrations and

ports included) and it was found that the TBR dropped to $1.0191 \pm 0.03\%$, $0.9892 \pm 0.03\%$, and $0.9513 \pm 0.03\%$ for 70%, 60%, and 50% Li^6 enrichment, respectively. The TBR satisfies the tritium breeding requirement of 1.04 with 80% Li^6 enrichment and the results are shown in figure 10.

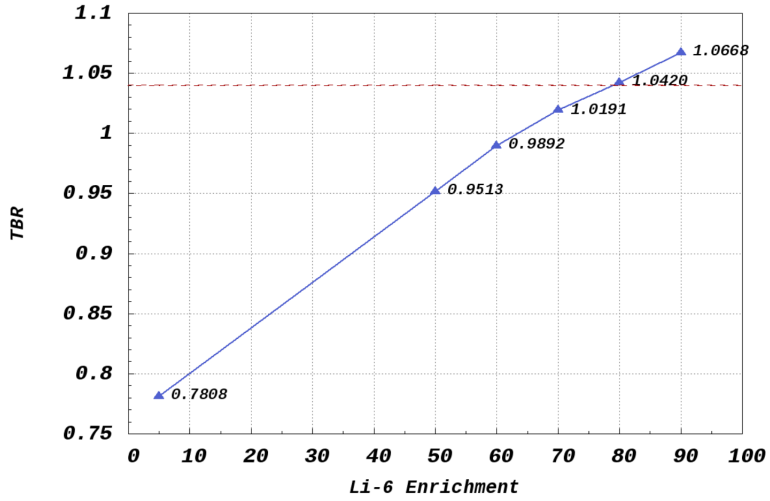

Figure 10: The facility overall TBR vs Li6 enrichment

4.4. TBR mapping

One of the concepts implemented in the current design – based on experience with previous models – is keeping the mid-plane clear of any ports/penetrations as practically achievable. The current model has a peak NWL of 1.75 and $1.31\,MW/m^2$ at the OB and IB mid-planes, respectively. This could directly be related to the calculated TBR (74% OB and 26% IB yield) showing that more T is produced near the mid-plane compared to the upper and lower (poloidal direction) or back (radial direction) of both the 0.5 m IB and the 1 m OB blankets.

Using DAG-MCNP5 mesh tally capabilities the T production was mapped in the IB and OB blankets of one sector as shown in figure 11 for step 7 and figure 12 for the NBI. Figure 11 also shows a reduction in TBR behind the stabilizing shells due to the absorption of neutrons by W. Including any penetrations in the mid-plane will have an effect on the overall TBR by reducing the active volume of the blanket where it's most effective for T

breeding, even though there may be slightly enhanced local T breeding far inside the blanket due to streaming of neutrons.

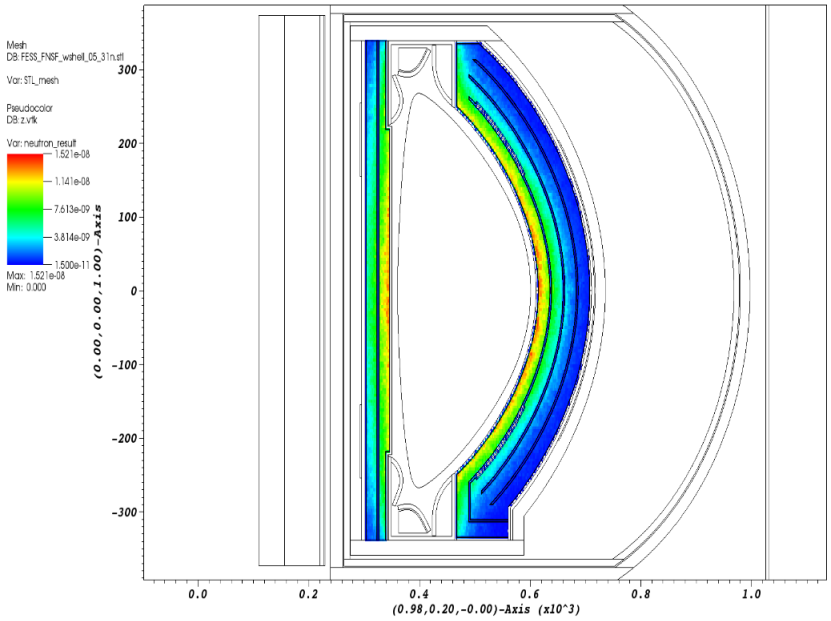

Figure 11: The tritium production mapping in one sector (without ports)

5. Radiation Damage

The shielding analysis followed the tritium breeding blanket optimization to provide the needed protection of the lifetime components. The main shielding design philosophy (as employed in previous designs [14]) is that every layer provides protection to the following layers such that collectively they would protect the out-of-vessel components such as the magnets. For example, in addition to the T breeding, the blanket (both the IB and OB) is supposed to provide protection for the structural ring and in turn both would protect the vacuum vessel and finally all three layers would attenuate the neutron and gamma fluxes to such low levels to protect the magnets. Such an approach requires some trade offs between compactness and performance to identify the optimal composition. An example would be the optimization of the VV, SR, and LT shield; the need for a compact IB radial build suggested the use of the WC filler for the SR, VV, and LT shield to

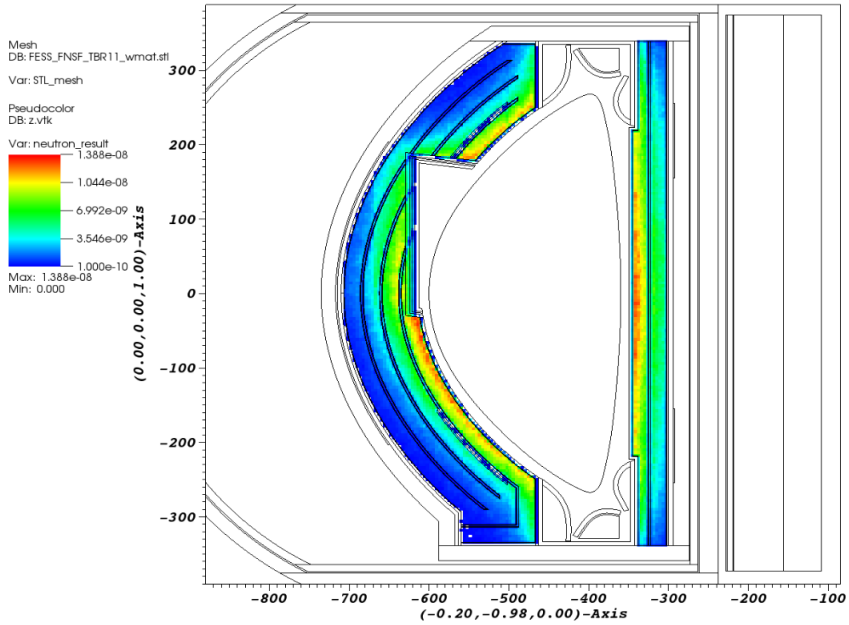

Figure 12: The tritium production mapping in one sector (with NBI)

reduce the major radius of the facility while the B-FS filler is limited to the OB and top/bottom sections of the SR and LT shield. Shown in figure 13 is a mapping of the neutron flux in the facility at the mid-plane (z=0) and from the figure it can be seen that a reduction of three orders of magnitude of the neutron flux across the OB breeding zone and SR is achieved. A detailed discussion of shielding optimization can be found in [2].

5.1. dpa, He/H production

The damage caused by irradiation to the in-vessel components is an important factor in the selection of materials in the design phase. The radiation damage can be quantified using two main parameters; displacement per atom (dpa) and gas (He and H) production. These parameters impact the lifetime of structural components and the potential for reweldability after irradiation.

For the FW, the peak values calculated at the mid-plane are shown in table 2. The radial distribution of the damage to the ferritic steel alloy (F82H) is shown in figure 14. It's worth noting that there is a slight increase in the He and H production near the end of the blanket at 700 cm due to

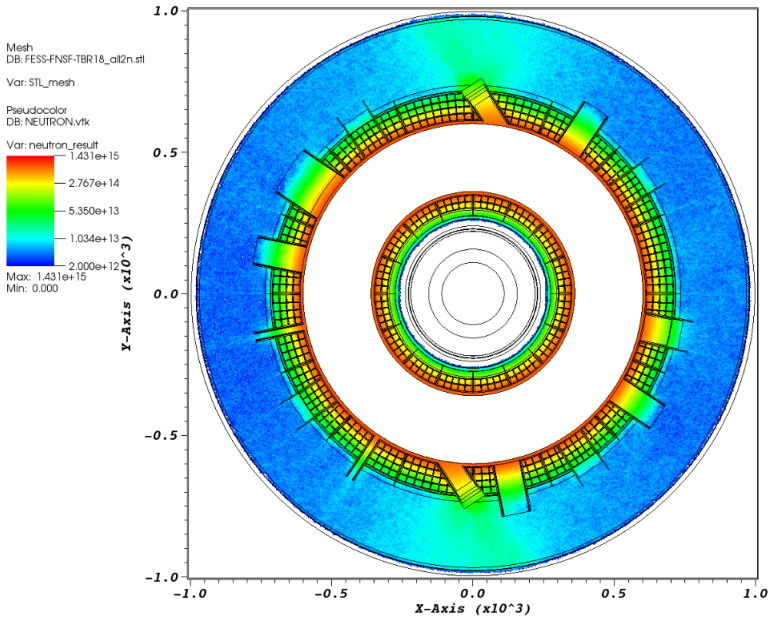

Figure 13: Mapping of the neutron flux at the mid-plane (z=0)

the strong neutron reflection from the SR/VV/shield. The reweldability of the VV is directly related to the levels of H and He produced during the operation and that leads to setting a limit of 1 He appm which shouldn't be exceeded at any time during plant operation. An issue that needs to be addressed is the streaming through the assembly gaps (2 cm between the OB and IB sectors) and all penetrations described in section 4.2 which will cause peaking in radiation damage to the exposed portions of the VV. The results of the damage at the VV mid-plane (away from the NBIs) are listed in table 2.

5.2. Magnet damage

The magnet is a critical component of the facility and is considered the main focus of all shielding optimization efforts. Following the shield design philosophy stated previously, the 3-D neutronics analysis confirmed that the radiation levels at the magnet winding pack (WP) met the limits set by the magnet designers. Calculations showed that the peak fast (E $>$ 0.1 MeV) neutron fluence at the WP $1.35\times10^{18} \pm 4.58\%$ n/cm^2 is well below the limit (5×10^{18} n/cm^2). The LT shield behind the VV has WC (37%) and H2O

Table 2: Radiation damage values for the FW and VV

	FW		VV	
	IB	OB	IB	OB
Damage [dpa/FPY]	13.70 ± 1.53%	15.25 ± 0.92%	0.1495 ± 0.64%	0.0114 ± 0.36%
He [appm/FPY]	137.30 ± 2.52%	154.58 ± 1.41%	0.3109 ± 8.83%	0.0029 ± 13.81%
He/dpa ratio	10.02	10.14	2.08	0.26
H [appm/FPY]	613.50 ± 2.42%	691.94 ± 1.35%	0.2462 ± 8.92%	0.0025 ± 12.99%

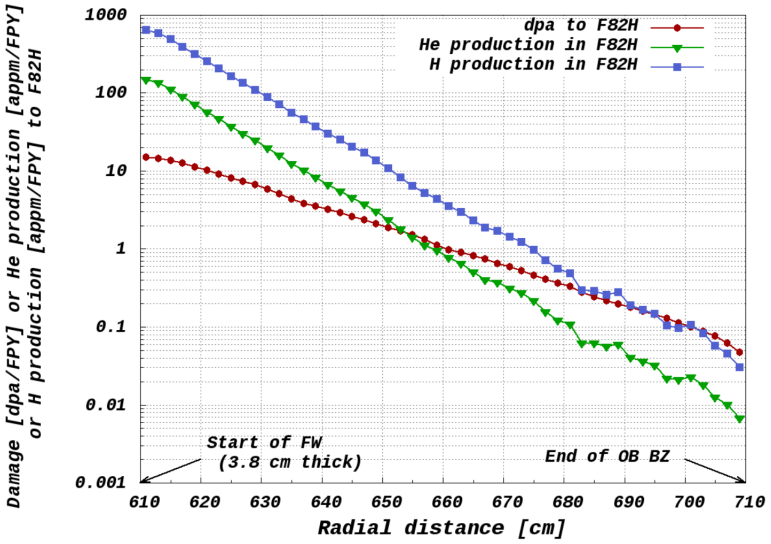

Figure 14: The radial distribution of radiation damage at OB

(33%) which combined have superior shielding capacity in attenuating the neutron flux. The peak nuclear heating at the coil case "CC" is 0.26 ± 2.55% mW/cm^3, below the limit of 2 mW/cm^3. The peak dpa to the Cu stabilizer is 9.54×10^{-5} ± 4.1% dpa/FPY, also below the limit of 10×10^{-4} dpa/FPY. The peak dose to the electrical insulator was also calculated and found to be 5.25×10^{8} ± 4.91% rads.

5.3. Total Heating

The total heating (neutron and gamma) was calculated for the model without any penetrations or ports inserted making use of the symmetry of all 16 sectors. Using DAG-MCNP5 the total heating tallies (F6) were calculated for all sub-volumes in one sector and the results were divided into 7 categories as shown in table 3. The regions are color-coded in figure 15 with the corresponding titles as appear on the table. The OB result is a sum of the heating over all regions from the FW up to the SR; OB FW, SW, BW, cooling channel, LiPb flow channels, liners, stabilizing shells, He manifold, and kink shell. The IB result is a sum over the corresponding regions on the IB; IB FW, SW, BW, cooling channel, LiPb flow channels, liners, stabilizing shells, and He manidfold. The heating was calculated for the three divertor plates both the top and bottom and the sum is given in the table and similarly for the dome shield and the box enclosing the divertors.

The total nuclear heating results for the stabilizing shells on the OB and IB are 0.8017 ± 0.4% and 0.055 ± 1.4% MW respectively. The total nuclear heating in all regions in the facility (all 16 sectors) = 475.7 MW which results in an energy multiplication factor (ratio of source neutron energy to total heating) of 1.15.

Table 3: Total (n+p) heating in all regions

	Neutron Heating [MW]	Gamma Heating [MW]	Total [MW]
Strucutral Ring "SR"	0.41 ± 0.18%	0.99 ± 0.42%	1.40 ± 0.30%
Divertor shield and Box	0.21 ± 0.31%	0.98 ± 0.43%	1.19 ± 0.36%
Divertor plates	0.09 ± 0.28%	1.75 ± 0.31%	1.84 ± 0.29%
Vacuum Vessel "VV"	0.03 ± 0.07%	0.15 ± 0.25%	0.18 ± 0.21%
LT shield	0.18 ± 0.06%	0.12 ± 0.25%	0.31 ± 0.11%
IB	3.51 ± 0.14%	2.83 ± 0.28%	6.34 ± 0.15%
OB	9.95 ± 0.10%	9.03 ± 0.17%	18.98 ± 0.10%

6. Shutdown Dose Rate Calculations

Part of the design effort of next step machines like the FESS-FNSF is dedicated to maintenance. The current design allows moving each sector of the 16 sectors individually through designed ports for purposes of maintenance

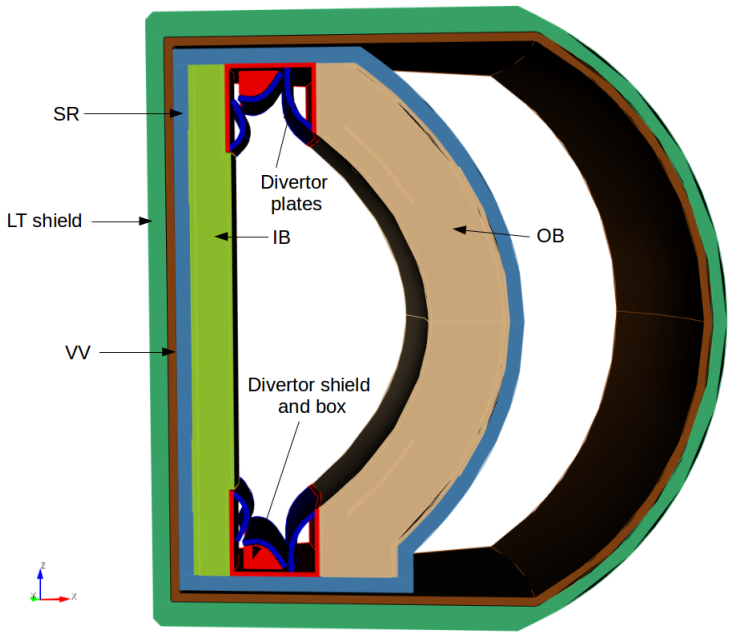

Figure 15: Definition of heating regions tabulated in table 3

or repair of components. An important question that needs to be aswered during the analysis phase of the design is the wait time after shutdown of the machine till the radiation levels are dropped below the allowed limits for personal access or handling outside the shield. To achieve such task, the calculation of the shutdown dose rate with high certainty, state-of-the-art tools were used. DAG-MCNP5 was used for photon transport and the activation code ALARA was used for nuclides inventory analysis and calculation of decay gamma source distribution.

6.1. Workflow

The shutdown dose rate is due to decay photons emitted by radioactive nuclides generated during operation from neutron interactions. The calculation of shutdown dose rate is achieved following three main steps; 1) Neutron transport calculation, 2) Nuclide inventory calculation, and 3) Decay gamma transport calculations.

Step (1) involved neutron transport calculation on the facility without any

ports or penetrations inserted which is believed to produce an upper bound for the radiation levels due to the fact that insertion of ports remove parts of the active volume of sectors leading to streaming to the outer VV and LT shield. Using meshtally capabiities of DAG-MCNP5 the spatial distribution of the neutron flux on a 6 cm × 6 cm × 6 cm mesh covering one sector of the 16 sectors was calculated. In step (2) the activation inventories and decay gamma sources (spectrum and intensity) were calculated for all regions in the sector using the corresponding materials along with the associated neutron flux spectra obtained in step (1). A simplified irradiation scenario was used; 0 s, 1 d, 2 d, 7 d, 14 d, 0.1 y, and 0.25 y.

The produced distribution of the decay gamma intensities in the mesh from step (2) is then used to produce the photon source distribution using the r2s module from the PyNE toolkit. The module produces a source file for each time step of the irradiation scenario which is then used for photon transport on the sector using DAG-MCNP5 totalling 7 calculations. Also for the purpose of clculating the temperature rise due to the desipated energy in the sector the heating due to the decay gamma energy deposition was calculated for each time step in the irradiation scenario.

6.2. SDR: results

6.3. Decay Heat: results

Table 4 gives the results of decay gamma heating in one sector at different times following the shutdown of the facility. The source strength at each time step was calculated using ALARA.

Table 4: Photon heating following shutdown

Time step	Decay gamma source intensity [p/s]	Photon heating [MW]
0 s	5.52×10^{19}	4.100 ± 0.04%
1 d	1.52×10^{19}	0.777 ± 0.07%
2 d	9.28×10^{18}	0.461 ± 0.06%
7 d	3.47×10^{18}	0.159 ± 0.05%
14 d	3.01×10^{18}	0.141 ± 0.05%
0.1 y	2.67×10^{18}	0.131 ± 0.05%
0.25 y	2.28×10^{18}	0.109 ± 0.05%

7. Conclusions

8. References

[1] C. E. KESSEL, et al., "The Fusion Nuclear Science Facility, the Critical Step in the Pathway to Fusion Energy," Fusion Science and Technology, vol. 68, p. 225–236 (2015).

[2] L. El-Guebaly, et al., "Design Approach for FESS-FNSF In-Vessel Components and Constraints Imposed on Radial/Vertical Build Definition," presented at 22nd ANS Topical Meeting on the Technology of Fusion Energy (TOFE), August 22 -25, 2016, Philadelphia, PA. To be published in Fusion Science and Technology.

[3] L. EL-GUEBALY et al., "Design and Evaluation of Nuclear System for ARIES-ACT2 Power Plant with DCLL Blanket," Fusion Science and Technology, in press.

[4] L. A. EL-GUEBALY, et al., "Toward the Ultimate Goal of Tritium Self-Sufficiency: Technical Issues and Requirements Imposed on ARIES Advanced Power Plants," Fusion Engineering and Design, vol. 84, p. 2072-2083 (2009).

[5] X-5 Monte Carlo Team, MCNP a General Monte Carlo N-Particle Transport Code Version 5, Tech. Rep. LA-CP-03-0245, Los Alamos National Laboratory, MCNP 5, (March 2005).

[6] DAGMC: http://svalinn.github.io/DAGMC/

[7] PyNE: http://pyne.io/

[8] D. L. ALDAMA and et al., "FENDL2.1, Update of an Evaluated Nuclear Data Library for Fusion applications." IAEA report INDC (NDS) 467, Vienna, Austria (2004).

[9] Y. Chen and U. Fischer, "Rigorous MCNP based shutdown dose rate calculations: computational scheme, verification calculations and application to ITER." Fusion Engineering and Design, 63-64, 107–114 (2002).

[10] pyne.r2s: http://pyne.io/pyapi/r2s.html

[11] https://github.com/svalinn/ALARA

[12] Clement Fausser, et al., "Tokamak D-T Neutron Source Models for Different Plasma Physics Confinement Modes." Fusion Engineering and Design, vol. 87, p. 787–792 (2012).

[13] S. MALANG et al., "Development of the Lead Lithium (DCLL) Blanket Concept," Fusion Science and Technology, 60, 249 (2011).

[14] L. EL-GUEBALY and the ARIES Team, "Overview of ARIES-RS Neutronics and Radiation Shielding: Key Issues and Main Conclusions," Fusion Engineering and Design, vol. 38, p. 139 – 158 (1997).